Journal of Alloys and Compounds 508 (2010) 570–581

Contents lists available at ScienceDirect

Journal of Alloys and Compounds

journal homepage: www.elsevier.com/locate/jallcom

Thermodynamic modeling of the Mg–Sn–Zn ternary system

F.G. Meng[a], J. Wang[b,*], L.B. Liu[c], Z.P. Jin[c]

[a] School of Materials Science and Engineering, Central South University of Forestry and Technology, Changsha, Hunan 410004, PR China
[b] EMPA, Swiss Federal Laboratories for Materials Testing and Research, Laboratory for Joining and Interface Technology, Überlandstrasse 129, Dübendorf, Zürich CH-8600, Switzerland
[c] School of Materials Science and Engineering, Central South University, Changsha, Hunan 410083, PR China

ARTICLE INFO

Article history:
Received 15 June 2010
Received in revised form 18 August 2010
Accepted 25 August 2010

Keywords:
Mg-based alloys
Phase diagram
CALPHAD
Mg–Sn–Zn ternary system

ABSTRACT

Mg-based alloys have been investigated widely due to the great potential for high performance structural applications. In the present work, the Mg–Sn binary system was re-optimized using the CALPHAD method through Thermo-calc® software package on the basis of available experimental information. Combined with the previous assessments of the Mg–Zn and Sn–Zn binary systems, the thermodynamic modeling of the Mg–Sn–Zn ternary system was performed. The liquid phase is described by the associated solution model with an associate Mg_2Sn, while the solid solution phases, hcp(Mg), bct(Sn) and hcp(Zn), are modeled by the substitutional solution model. The intermetallic compound Mg_2Sn is treated as a stoichiometric compound and its Gibbs energy was assessed considering the experimental heat capacity and heat content. The solubility of Sn in the Mg–Zn intermetallic compounds, Mg_7Zn_3, MgZn, Mg_2Zn_3, $MgZn_2$ and Mg_2Zn_{11}, is not taken into account. Liquidus projection and many vertical sections of this ternary system were calculated. The calculated results are in good agreement with the reported experimental data.

1. Introduction

Mg-based alloys have great potential for high performance structural applications in the automotive and aerospace industries due to their good properties such as low density, high specific strength, superior damping capacity and good castability [1–9]. For example, Mg–Zn-based alloys as the casting and wrought Mg alloys have been developed, which exhibit high strength and hardness followed by the typical heat treatment [1–3]. On the other hand, Mg–Sn-based alloys have been investigated actively to develop novel Mg-based alloys with the stable structure and good mechanical properties at the high temperature [4–6]. However, there are a number of undesirable properties such as poor corrosion resistance, inferior creep resistance and poor plastic processing ability, resulting in the limited applications of the Mg-based alloys. Therefore, increasing efforts have been made to develop Mg-based alloys with the excellent performances through addition of rare earth elements and other alloying elements (such as Al, Ca, Cu, Sr, Si, Sn, Y, Zn and Zr) as well as optimization of the heat treatment and processing [1–9]. In order to better understand the role of alloying elements and to design alloy compositions, phase diagrams and thermodynamic properties of the related Mg-based alloy systems are indispensable [7–9].

As mentioned above, the Mg–Sn–Zn ternary system has become one of the most important Mg-based alloy systems. Bamberger [10] calculated the Mg–Sn–Zn ternary system from the extrapolation of the three binary sub-systems using a commercial Mg database, but the experimental information of this ternary system in published literature was not reviewed. Thermodynamic calculation of the Mg–Sn–Zn ternary system was also carried out by Jung et al. [11] using the FactSage software. However, the complete thermodynamic modelling of the Mg–Sn–Zn ternary system has not reported in Refs. [10,11]. Therefore, the present work is to evaluate the experimental phase diagram and thermodynamic data of the Mg–Sn binary system using the CALPHAD method [12,13] and Thermo-calc® software package [14] and to obtain a consistent and reliable thermodynamic description of the Mg–Sn–Zn ternary system in combination with the previous assessments of the Mg–Zn and Sn–Zn binary systems.

2. Binary systems

2.1. The Mg–Zn binary system

The Mg–Zn binary system was assessed by Agarwal et al. [15], which reproduced most experimental information on thermodynamic properties and phase boundaries. The updated optimization of this binary system was carried out by Liang et al. [16] based on the modification of thermodynamic models and the new experimental data in the assessment of the Al–Mg–Zn ternary system.

* Corresponding author. Tel.: +41 44 823 4250.
E-mail addresses: wangjiang158@gmail.com, jiang.wang@empa.ch (J. Wang).

0925-8388/$ – see front matter © 2010 Elsevier B.V. All rights reserved.
doi:10.1016/j.jallcom.2010.08.124

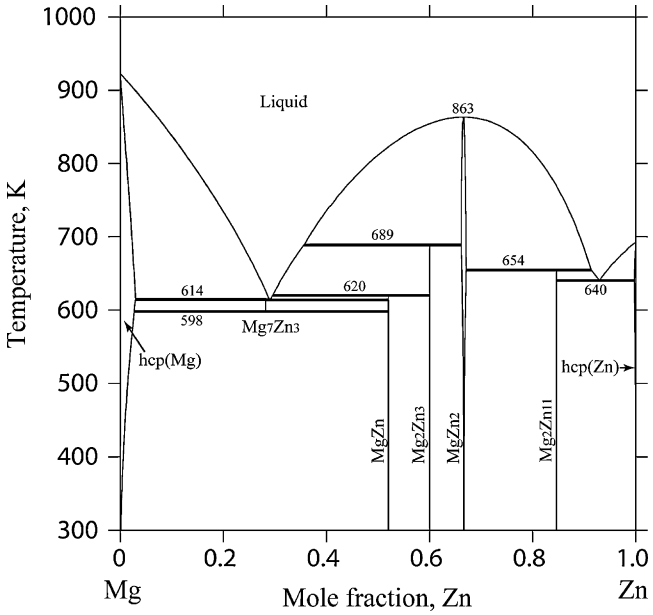

Fig. 1. Calculated phase diagram of the Mg–Zn binary system by Liang et al. [16].

Furthermore, this assessment was also used in the extrapolation of the Cu–Mg–Zn [17], Mg–Mn–Zn [18] and Mg–La–Zn [19] ternary systems. Thus, the Gibbs energies of various phases in the Mg–Zn binary system obtained by Liang et al. [16] were employed directly in the present work. Fig. 1 shows the calculated phase diagram of the Mg–Zn binary system.

2.2. The Sn–Zn binary system

Lee [20] assessed firstly the Sn–Zn binary system in their serial assessments of Pb-free solder alloys. Afterwards, Ohtani et al. [21] employed the different lattice stability of hcp-Sn to optimize this binary system. Considering the compatibility of thermodynamic database in the multi-component system, the assessment of Lee [20] was used in the present work. The calculated phase diagram of the Sn–Zn binary system is presented in Fig. 2.

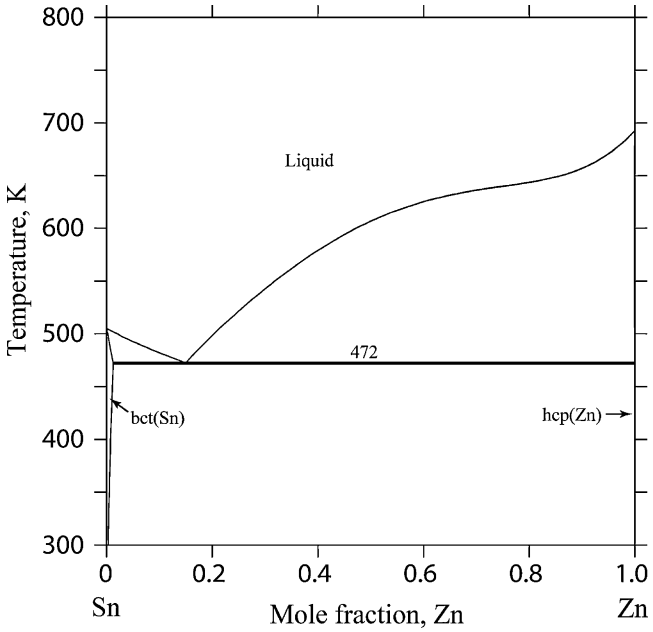

Fig. 2. Calculated phase diagram of the Sn–Zn binary system by Lee [20].

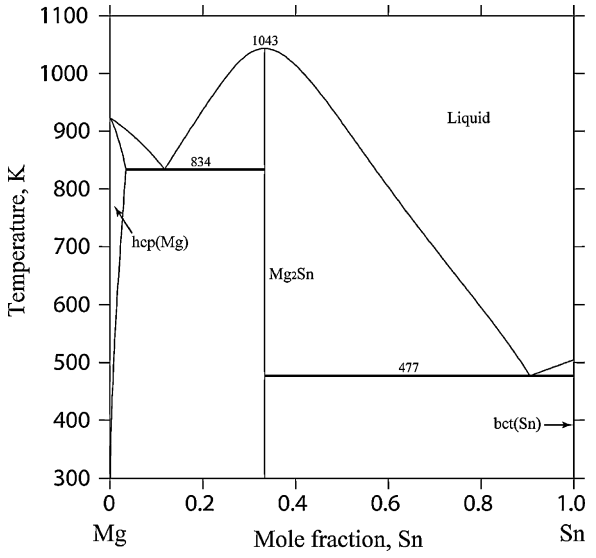

Fig. 3. Calculated phase diagram of the Mg–Sn binary system in the present work.

2.3. The Mg–Sn binary system

The Mg–Sn binary system was reviewed critically by Nayeb-Hashemi and Clark [22] up to 1984. Fries and Lukas [23] assessed this binary system based on the reported experimental information. However, the inadvertent stability of the hcp(Mg) phase was not noticed, which is stable in Sn-rich side in the original publication. The optimization of this binary system was updated later, but the complete thermodynamic parameters of all condensed phases were not published in Ref. [24]. In addition, the new experimental data on the heat capacity and heat content of Mg_2Sn at low temperature were reported recently. Therefore, the re-assessment of the Mg–Sn binary system was carried out in the present work based on the reported experimental data and previous optimizations [23,24].

3. Experimental information

3.1. The Mg–Sn binary system

The Mg–Sn binary system was investigated by many researchers [25–36]. Heycock and Neville [25] determined firstly the liquids of the bct(Sn) phase through

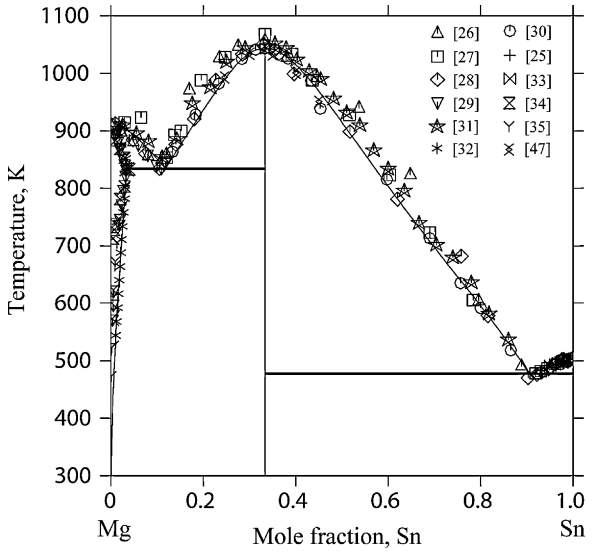

Fig. 4. Calculated phase diagram of the Mg–Sn binary system compared with the experimental data [26–35,47] in the present work.

measuring the effect of Mg on the freezing point of molten Sn. Afterwards, the liquidus was determined by Grube [26], Kurnakow and Stepanow [27], Hume-Rothery [28], Raynor [29] and Steiner et al. [30] using thermal analysis as well as by Nayak and Oelsen [31,32] using calorimetry. Also, Ellmer et al. [33] reported the liquidus in the Sn-rich side. There are some slight discrepancies for the measured liquidus of the hcp(Mg) phase and intermetallic compound Mg_2Sn, while the reported that of the bct(Sn) phase are in good agreement with each other. After analyzed carefully these experimental data [25–33], Nayeb-Hashemi and Clark [22] pointed out that the experimental results of Hume-Rothery [28], Raynor [29] and Steiner et al. [30] are much more reliable than others. This conclusion was accepted in the present work. The phase boundary of the hcp(Mg) phase was measured by Grube and Vosskühler [34] and Vosskühler [35] using resistivity analysis, by Raynor [29] using metallography, by Nayak and Oelsen [32] using calorimetry, and by Nishinura and Tanaka [36] using heat tinting method. The solidus measured by Raynor [29], Nayak and Oelsen [32], Grube and Vosskühler [34] and Vosskühler [35] are in mutual agreement, whereas the solubility of Sn in the hcp(Mg) phase measured by Nayak and Oelsen [32] is slight higher than those of Vosskühler [35] and Raynor [28]. The experimental information mentioned above was taken into account in the present optimization.

According to the review [22], the solubility of Mg in bct(Sn) phase appears to be very small and thus was ignored during the present optimization. In addition, the intermetallic compound Mg_2Sn is treated as a stoichiometric compound in the present work because its homogeneity of Mg_2Sn is very narrow.

Enthalpy of mixing of liquid Mg–Sn alloys was determined by Kawakami [37] at 1073 K, Nayek and Oelsen [38] at 1073 K and Sommer et al. [39] at 1073 K, 1133 K and

Table 1
Thermodynamic parameters of the Mg–Sn–Zn ternary system.

Phase	Thermodynamic parameters[a]	Reference
Liquid (Mg, Mg_2Sn, Sn, Zn)	${}^{(0)}L^{L}_{Mg,Zn} = -77729.24 + 680.52266T - 95T\ln T + 0.04T^2$	[16]
	${}^{(1)}L^{L}_{Mg,Zn} = +3674.72 + 0.57139T$	
	${}^{(2)}L^{L}_{Mg,Zn} = -1588.15$	
	${}^{(0)}L^{L}_{Sn,Zn} = +12558 - 8.7041T$	[20]
	${}^{(1)}L^{L}_{Sn,Zn} = -5623 + 4.196T$	
	${}^{(2)}L^{L}_{Sn,Zn} = +4149 - 4.091T$	
	${}^{0}G^{L}_{Mg_2Sn} = -66092.9 + 94.809T - 11.576T\ln T + 2{}^{0}G^{L}_{Mg} + {}^{0}G^{L}_{Sn}$	This work
	${}^{(0)}L^{L}_{Mg,Mg_2Sn} = +5970.6 - 8.744T$	
	${}^{(0)}L^{L}_{Mg,Sn} = -30841.1 + 0.781T$	
	${}^{(0)}L^{L}_{Mg_2Sn,Sn} = -12468.2 - 4.815T$	
	${}^{(0)}L^{L}_{Mg_2Sn,Zn} = +9000 - 4.3T$	This work
	${}^{(0)}L^{L}_{Mg,Sn,Zn} = +20000 - 35T$	
	${}^{(1)}L^{L}_{Mg,Sn,Zn} = +25000 - 30T$	
	${}^{(2)}L^{L}_{Mg,Sn,Zn} = +78000 - 92T$	
hcp(Mg) (Mg, Sn, Zn)	${}^{0}G^{hcp\_A3}_{Zn} = {}^{0}G^{hcp\_Zn}_{Zn} + 2969.82 - 1.56968T$	[16]
	${}^{(0)}L^{hcp}_{Mg,Zn} = -3056.82 + 5.63801T$	
	${}^{(1)}L^{hcp}_{Mg,Zn} = -3127.26 + 5.65563T$	
	${}^{(0)}L^{hcp}_{Sn,Zn} = +30453$	[20]
	${}^{(0)}L^{hcp}_{Mg,Sn} = -26256.5 + 6.234T$	This work
	${}^{(1)}L^{hcp}_{Mg,Sn} = -31895.7$	
hcp(Zn) (Mg, Sn, Zn)	${}^{0}G^{hcp\_Zn}_{Mg} = {}^{0}G^{hcp\_A3}_{Mg} + 100$	[16]
	${}^{(0)}L^{hcp\_Zn}_{Mg,Zn} = -3056.82 + 5.63801T$	
	${}^{(1)}L^{hcp\_Zn}_{Mg,Zn} = -3127.26 + 5.65563T$	
	${}^{(0)}L^{hcp\_Zn}_{Sn,Zn} = +30453$	[16]
	${}^{(0)}L^{hcp\_Zn}_{Mg,Sn} = +8000$	This work
bct(Sn) (Sn, Zn)	${}^{0}G^{bct}_{Zn} = {}^{0}G^{hcp\_Zn}_{Zn} + 4184$	[20]
	${}^{(0)}L^{bct}_{Sn,Zn} = +6660 + 19.686T$	
Mg_7Zn_3 $(Mg)_7(Zn)_3$	$G^{Mg_7Zn_3} = 7{}^{0}G^{hcp\_A3}_{Mg} + 3{}^{0}G^{hcp\_Zn}_{Zn} - 335741.54 + 35.5T$	[16]
MgZn $(Mg)_1(Zn)_1$	$G^{MgZn} = 12{}^{0}G^{hcp\_A3}_{Mg} + 13{}^{0}G^{hcp\_Zn}_{Zn} - 236980.84 + 59.24524T$	[16]
Mg_2Zn_3 $(Mg)_2(Zn)_3$	$G^{Mg_2Zn_3} = 2{}^{0}G^{hcp\_A3}_{Mg} + 3{}^{0}G^{hcp\_Zn}_{Zn} - 54406.2 + 13.60156T$	[16]
$MgZn_2$ (Mg, Zn)$_1$(Mg, Zn)$_2$	${}^{0}G^{MgZn_2}_{Mg:Mg} = 3{}^{0}G^{hcp\_A3}_{Mg} + 15000$	[16]
	${}^{0}G^{MgZn_2}_{Mg:Zn} = {}^{0}G^{hcp\_A3}_{Mg} + 2{}^{0}G^{hcp\_Zn}_{Zn} - 35355.45 + 8.83886T$	
	${}^{0}G^{MgZn_2}_{Zn:Mg} = 2{}^{0}G^{hcp\_A3}_{Mg} + {}^{0}G^{hcp\_Zn}_{Zn} + 65355.45 - 8.83886T$	
	${}^{0}G^{MgZn_2}_{Zn:Zn} = 3{}^{0}G^{hcp\_Zn}_{Zn} + 15000$	
	${}^{(0)}L^{MgZn_2}_{Mg,Zn:Mg} = {}^{(0)}L^{MgZn_2}_{Mg,Zn:Zn} = +8000$	
	${}^{(0)}L^{MgZn_2}_{Mg:Mg,Zn} = {}^{(0)}L^{MgZn_2}_{Zn:Mg,Zn} = +35000$	
Mg_2Zn_{11} $(Mg)_2(Zn)_{11}$	$G^{Mg_2Zn_{11}} = 2{}^{0}G^{hcp\_A3}_{Mg} + 11{}^{0}G^{hcp\_Zn}_{Zn} - 73818.32 + 18.45457T$	[16]
Mg_2Sn $(Mg)_2(Sn)_1$	$G^{Mg_2Sn} = -96165.9 + 339.999T - 66.285T\ln T - 0.0121662T^2 + 96000T^{-1} + 3.33828\times10^{-7}T^3$	This work

[a] Gibbs energies are expressed in J/mol. The all lattice stabilities of Mg, Sn and Zn are given by Dinsdale [58].

Table 2
Invariant reactions in the Mg–Sn binary system.

Invariant reaction	Type	T (K)	Composition (x^L_{Sn})	Reference
$L \leftrightarrow hcp(Mg) + Mg_2Sn$	Eutectic	838	0.116	[26]
		854	0.120	[27]
		834	0.105	[28]
		834	0.107	[29]
		839	0.105	[31]
		840	0.107	[32]
		834	0.110	[30]
		833	–	[34]
		834	–	[35]
		834	0.112	[23]
		834	0.118	This work
$L \leftrightarrow Mg_2Sn$	Congruent	1056	0.333	[26]
		1068	0.333	[27]
		1051	0.333	[28]
		1053	0.333	[31]
		1051	0.333	[32]
		1044	0.333	[30]
		1043	0.333	[46]
		1043	0.333	[45]
		1043	0.333	[23]
		1043	0.333	This work
$L \leftrightarrow Mg_2Sn + bct(Sn)$	Eutectic	482	0.889	[26]
		477	0.915	[27]
		473	0.903	[28]
		471	0.914	[31]
		471	0.914	[32]
		476	0.904	[30]
		476	0.908	[23]
		477	0.905	This work

1213 K using calorimetry. The calculated enthalpy of mixing of liquid Mg–Sn alloys was also reported by Eremenko and Lukashenko [40] at 923 K from the electromotive force (EMF) measurements as well as by Steiner et al. [30] at 1043 K, Eldridge et al. [41] at 1043 K and Sharma [42] at 1073 K from the vapor pressure measurements. It is evident that the measured enthalpy of mixing of liquid alloys by Nayek and Oelsen [38] at 1073 K is less negative than the data obtained by Kawakami [37] and Sommer et al. [39]. The enthalpies of mixing of liquid alloys at three different temperatures from Sommer et al. [39] show slight temperature dependency in the composition range of 30–50 at.% Sn. Thus, the dependence of the enthalpy of mixing of the liquid alloys on temperature is taken into account. Moreover, it should be pointed out that the enthalpy of mixing deduced from electromotive force and vapour pressure methods may be not as reliable as the data obtained directly through calorimetry. Therefore, the experimental data in Refs. [37,39] were used in the present optimization, while the results in Refs. [38,40–42] were given up and only compared with the present calculated results.

The activity of Mg in liquid Mg–Sn alloys was determined by Eldridge et al. [43] and Ashatakala and Pidgeon [44] by the vapor pressure method as well as by Eremenko and Lukashenko [40], Sharma [42], Eckert et al. [45], Egan [46] and Moser et al. [47] through the EMF method. In the present work, the experimental data on activity of Mg in liquid Mg–Sn alloys in Refs. [42,45–47] was used.

The enthalpies of formation of the solid Mg–Sn alloys were determined by Kubaschewski [48] at 923 K, Nayak and Oelsen [49] at 293 K and Borsese et al. [50] at 300 K, respectively. The enthalpy of formation of Mg_2Sn was measured by Kubaschewski and Evans [51], Beadmore et al. [52] and Sommer et al. [39]. In addition, the heat capacity of Mg_2Sn in the temperature from 2 K to 300 K was determined by Jelinek et al. [53] and Morishita and Koyama [54]. Moreover, the heat contents (H_T–H_{298}) of Mg_2Sn were reported by Sommer et al. [39] in high temperature range and by Morishita and Koyama [54] in low temperature range. The experimental results [39,48–54] are consistent with each other and thus were considered in the present optimization.

Table 3
Invariant reactions in the Mg–Sn–Zn ternary system.

Invariant reaction	Type	T (K)	Composition		Reference
			(x^L_{Mg})	(x^L_{Zn})	
$L \leftrightarrow Mg_2Sn + MgZn_2$	e_1	843	0.3805	0.5729	[56]
		840	0.3859	0.5658	[57]
		837	0.3880	0.5569	This work
$L \leftrightarrow Mg_2Sn + hcp(Zn)$	e_2	626	0.0976	0.8511	[56]
		628	0.0894	0.8691	[57]
		625	0.0761	0.8783	This work
$L + MgZn_2 \leftrightarrow Mg_2Sn + Mg_2Zn_3$	U_1	684	0.6475	0.3405	This work
$L + Mg_2Zn_3 \leftrightarrow Mg_2Sn + MgZn$	U_2	618	0.7049	0.2902	This work
$L + Mg_2Sn \leftrightarrow hcp(Mg) + MgZn$	U_3	614	0.7081	0.2873	This work
$L + MgZn_2 \leftrightarrow Mg_2Sn + Mg_2Zn_{11}$	U_4	641	0.0969	0.8641	[57]
		644	0.0951	0.8788	This work
$L \leftrightarrow hcp(Mg) + MgZn + Mg_7Zn_3$	E_1	614	0.7097	0.2896	This work
$L \leftrightarrow Mg_2Sn + Mg_2Zn_{11} + hcp(Zn)$	E_2	626	0.0917	0.8691	[57]
		624	0.0771	0.8798	This work
$L \leftrightarrow Mg_2Sn + bct(Sn) + hcp(Zn)$	E_3	456	0.0739	0.1147	[57]
		459	0.0653	0.1005	This work

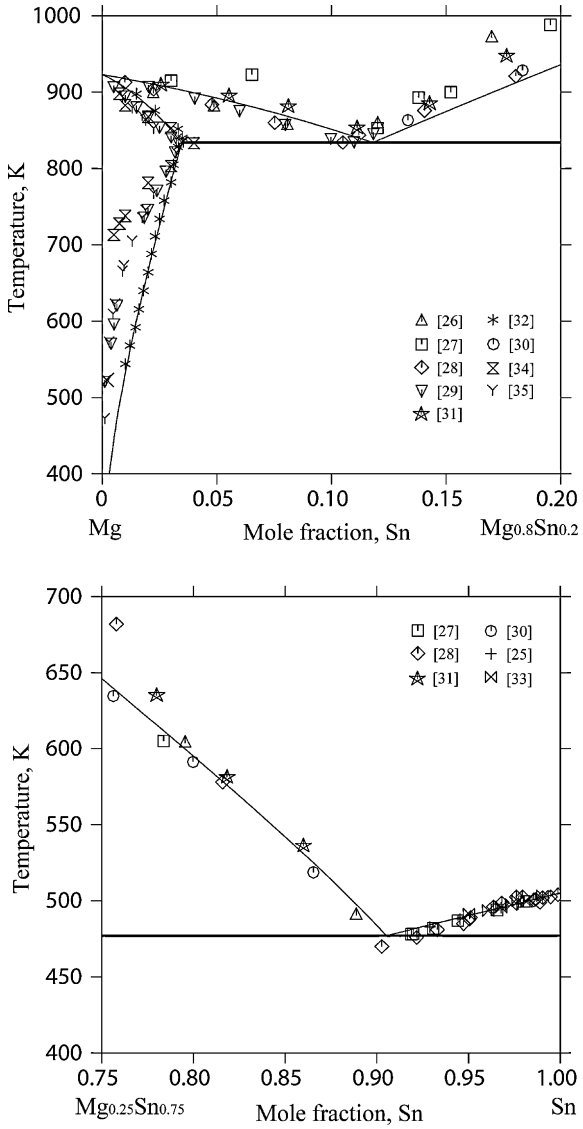

Fig. 5. Enlarged phase diagram of the Mg–Sn binary system with the experimental data [26–35] in the present work. (a) Mg-rich part and (b) Sn-rich part.

3.2. The Mg–Sn–Zn ternary system

Ogawa et al. [55] studied experimentally the liquid Mg–Sn–Zn alloys in the temperature range from 700 K to 800 K using a mass spectrometer. No experimental values for activities of components and excess Gibbs energy of liquid alloys were determined in their work. Furthermore, it should be pointed out that the compositions of alloy samples were changed because of Zn evaporation during their experiments. Therefore, their experimental information is not reliable and was not taken into account in the present optimization. Except for Ref. [55], thermodynamic properties of the Mg–Sn–Zn ternary system have been not reported in the published literature.

Using the thermal analysis and microscopy method, Otani [56] studied the phase relations of the Mg–Sn–Zn ternary system. Five vertical sections, 2 wt.% Mg, 48 wt.% Mg, 2 wt.% Sn, 10 wt.% Sn and 3 wt.% Zn, were determined, respectively. The Mg_2Sn–$MgZn_2$ and Mg_2Sn–Zn vertical sections were also measured as pseudobinary eutectic systems. It should be noted that Otani [56] constructed and analyzed these vertical sections and invariant reactions based on the outdated phase diagram of the Mg–Zn binary system including only four intermetallic compounds, η (about 30 at.% Zn), MgZn, $MgZn_2$ and $MgZn_5$. However, five intermetallic compounds, Mg_7Zn_3, MgZn, Mg_2Zn_3, $MgZn_2$ and Mg_2Zn_{11}, were confirmed experimentally in the updated Mg–Zn phase diagram. Recently, Gödecke and Sommer [57] investigated the Mg_2Sn–$MgZn_2$–Zn–Sn part in the Mg–Sn–Zn ternary system through the thermal analysis and microscopy method. Six vertical sections, 10 wt.% Mg, 2 wt.% Sn, 40 wt.% Sn, 85 wt.% Sn, 70 wt.% Zn and 90 wt.% Zn, were measured, respectively. The $MgZn_2$–Mg_2Sn and Zn–Mg_2Sn vertical sections were also verified to be pseudobinary eutectic systems. The invariant reactions and liquid projection for the Mg_2Sn–$MgZn_2$–Zn–Sn part were established.

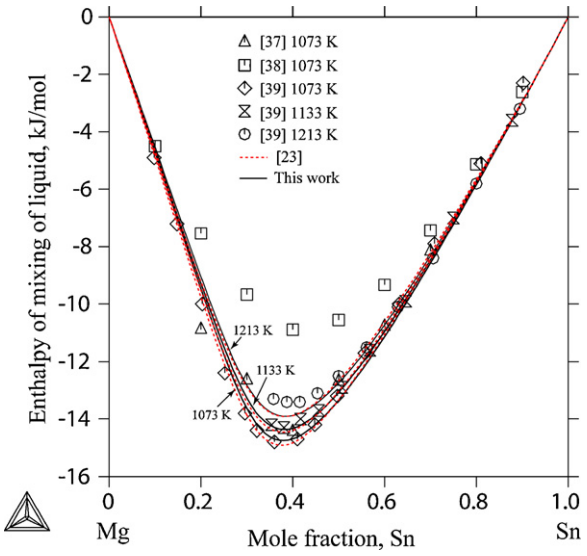

Fig. 6. Calculated enthalpies of mixing of liquid alloys in comparison with experimental data [37–39] and the assessed results [23] (Ref. states: liquid Mg and liquid Sn).

According to the measurements by Otani [56] and Gödecke and Sommer [57], no stable ternary compound was found in the Mg–Sn–Zn system. The experimental information on the phase relations in Refs. [56,57] was taken into account in the present optimization.

4. Thermodynamic model

4.1. Pure elements

The stable forms of the pure elements at 298.15 K and 1 bar are chosen as the reference states. The Gibbs energy for the element i in ϕ status is given as:

$$ {}^{0}G_i^{\phi}(T) = G_i^{\phi}(T) - H_i^{SER} = a + b\cdot T + c\cdot T\ln T + d\cdot T^2 + e\cdot T^3 + f\cdot T^{-1} + g\cdot T^7 + h\cdot T^{-9} \quad (1) $$

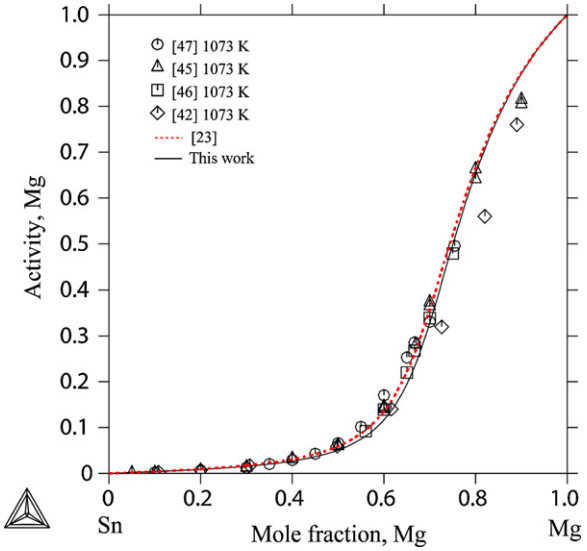

Fig. 7. Calculated activity of Mg at 1073 K with the experimental data [42,45–47] and the assessed results [23] (Ref. state: liquid Mg).

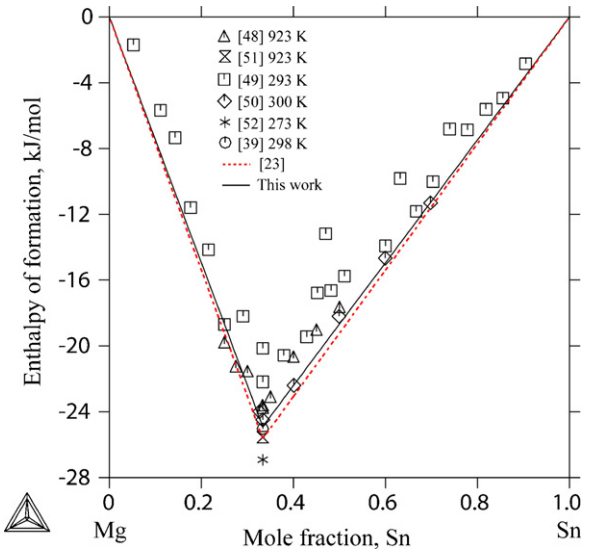

Fig. 8. Calculated enthalpies of formation of solid in comparison with the experimental data [39,48–52] and the assessed results [23] at 298 K (Ref. states: hcp-Mg and bct-Sn).

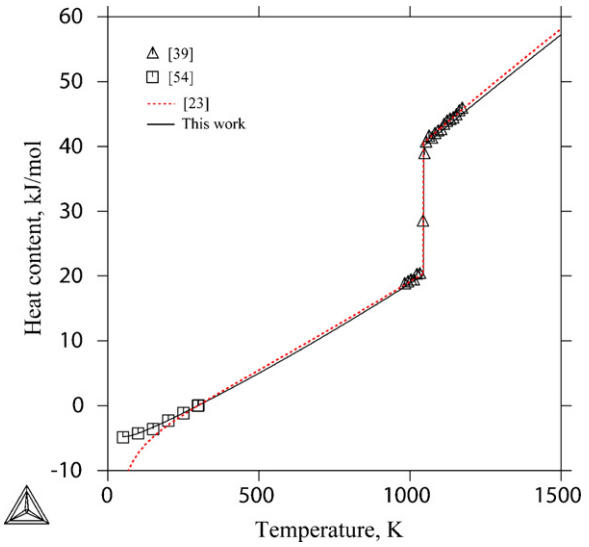

Fig. 10. Calculated heat content of Mg_2Sn in comparison with the experimental data [39,54] and the assessed results [23].

where H_i^{SER} is the enthalpy of the element i in its standard reference state (SER) at 298.15 K and 1 bar; T is the absolute temperature in K; $G_i^{\phi}(T)$ is the Gibbs energy of the element i with structure ϕ; ${}^0G_i^{\phi}(T)$ is the molar Gibbs energy of the element i with the structure of ϕ referred to the enthalpy of its stable state at 298.15 K and 1 bar. In the present work, ${}^0G_{Mg}^{\phi}(T)$, ${}^0G_{Sn}^{\phi}(T)$ and ${}^0G_{Zn}^{\phi}(T)$ are taken from the SGTE (Scientific Group Thermodata Europe) database compiled by Dinsdale [58].

4.2. Liquid and solution phases

The liquid phase is described using the associate solution model based on the experimentally measurements of mixing enthalpy of the Mg–Sn liquid alloys. The liquid phase is assumed to be constitute of four species: Mg, Sn, Zn and Mg_2Sn. Review and description of the associate model can be found in Refs. [59,60]. The molar Gibbs energy of the liquid phase is described by:

$$G_m^L = y_{Mg}\,{}^0G_{Mg}^L + y_{Sn}\,{}^0G_{Sn}^L + y_{Zn}\,{}^0G_{Zn}^L + y_{Mg_2Sn}\,{}^0G_{Mg_2Sn}^L + RT(y_{Mg}\ln y_{Mg} + y_{Sn}\ln y_{Sn} + y_{Zn}\ln y_{Zn} + y_{Mg_2Sn}\ln y_{Mg_2Sn}) + {}^EG_m^L \quad (2)$$

and

$$\begin{aligned} {}^EG_m^L = {} & y_{Mg}y_{Sn}\sum_{i=0}^{n}{}^{(i)}L_{Mg,Sn}^L(y_{Mg}-y_{Sn})^i \\ & + y_{Mg}y_{Mg_2Sn}\sum_{i=0}^{n}{}^{(i)}L_{Mg,Mg_2Sn}^L(y_{Mg}-y_{Mg_2Sn})^i \\ & + y_{Mg_2Sn}y_{Sn}\sum_{i=0}^{n}{}^{(i)}L_{Mg_2Sn,Sn}^L(y_{Mg_2Sn}-y_{Sn})^i \\ & + y_{Mg}y_{Zn}\sum_{i=0}^{n}{}^{(i)}L_{Mg,Zn}^L(y_{Mg}-y_{Zn})^i \\ & + y_{Sn}y_{Zn}\sum_{i=0}^{n}{}^{(i)}L_{Sn,Zn}^L(y_{Sn}-y_{Zn})^i \\ & + y_{Mg_2Sn}y_{Zn}\sum_{i=0}^{n}{}^{(i)}L_{Mg_2Sn,Zn}^L(y_{Mg_2Sn}-y_{Zn})^i \\ & + y_{Mg}y_{Mg_2Sn}y_{Sn}L_{Mg,Mg_2Sn,Sn}^L + y_{Mg}y_{Mg_2Sn}y_{Zn}L_{Mg,Mg_2Sn,Zn}^L \\ & + y_{Mg_2Sn}y_{Sn}y_{Zn}L_{Mg_2Sn,Sn,Zn}^L + y_{Mg}y_{Mg_2Sn}y_{Sn}y_{Zn}L_{Mg,Mg_2Sn,Sn,Zn}^L \\ & + x_{Mg}x_{Sn}x_{Zn}L_{Mg,Sn,Zn}^L \end{aligned} \quad (3)$$

with

$${}^0G_{Mg_2Sn}^L = a_0 + b_0\cdot T + c_0\cdot T\ln T + 2\,{}^0G_{Mg}^L + {}^0G_{Sn}^L \quad (4)$$

$$L_{Mg,Sn,Zn}^L = x_{Mg}{}^{(0)}L_{Mg,Sn,Zn}^L + x_{Sn}{}^{(1)}L_{Mg,Sn,Zn}^L + x_{Zn}{}^{(2)}L_{Mg,Sn,Zn}^L \quad (5)$$

where y_i (i = Mg, Mg_2Sn, Sn and Zn) represents the mole fraction of each species in the liquid phase; ${}^{(i)}L_{Mg,Sn}^L$, ${}^{(i)}L_{Mg,Mg_2Sn}^L$, ${}^{(i)}L_{Mg_2Sn,Sn}^L$, ${}^{(i)}L_{Mg,Mg_2Sn,Sn}^L$, ${}^{(i)}L_{Mg,Zn}^L$ and ${}^{(i)}L_{Sn,Zn}^L$ are interaction

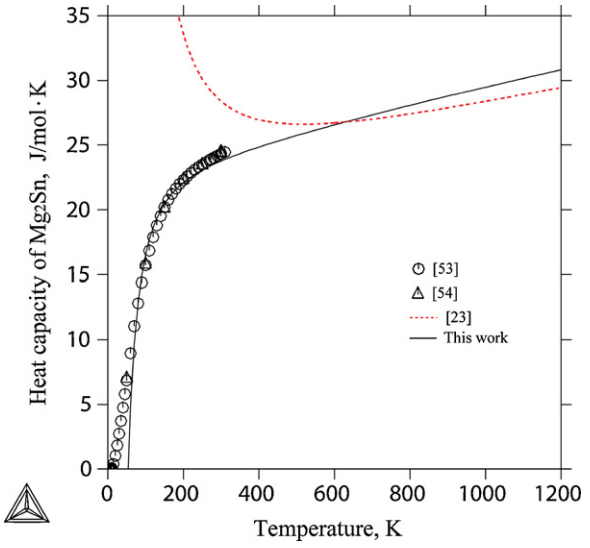

Fig. 9. Calculated heat capacity of Mg_2Sn in comparison with the experimental data [53,54] and the assessed results [23].

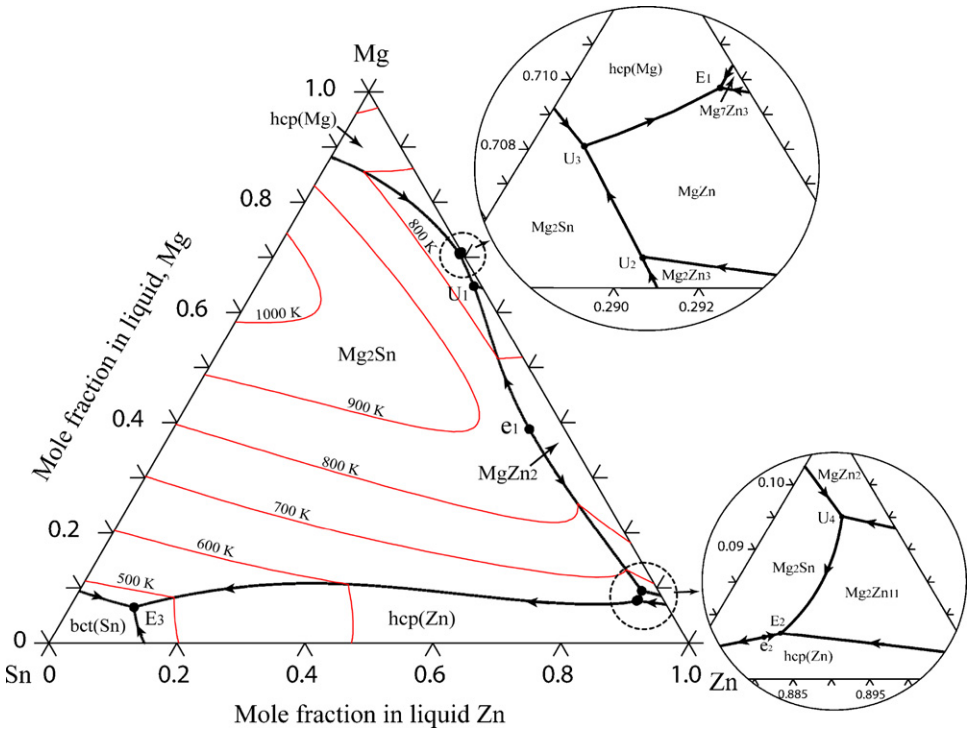

Fig. 11. Calculated liquid projection of the Mg–Sn–Zn ternary system in the present work.

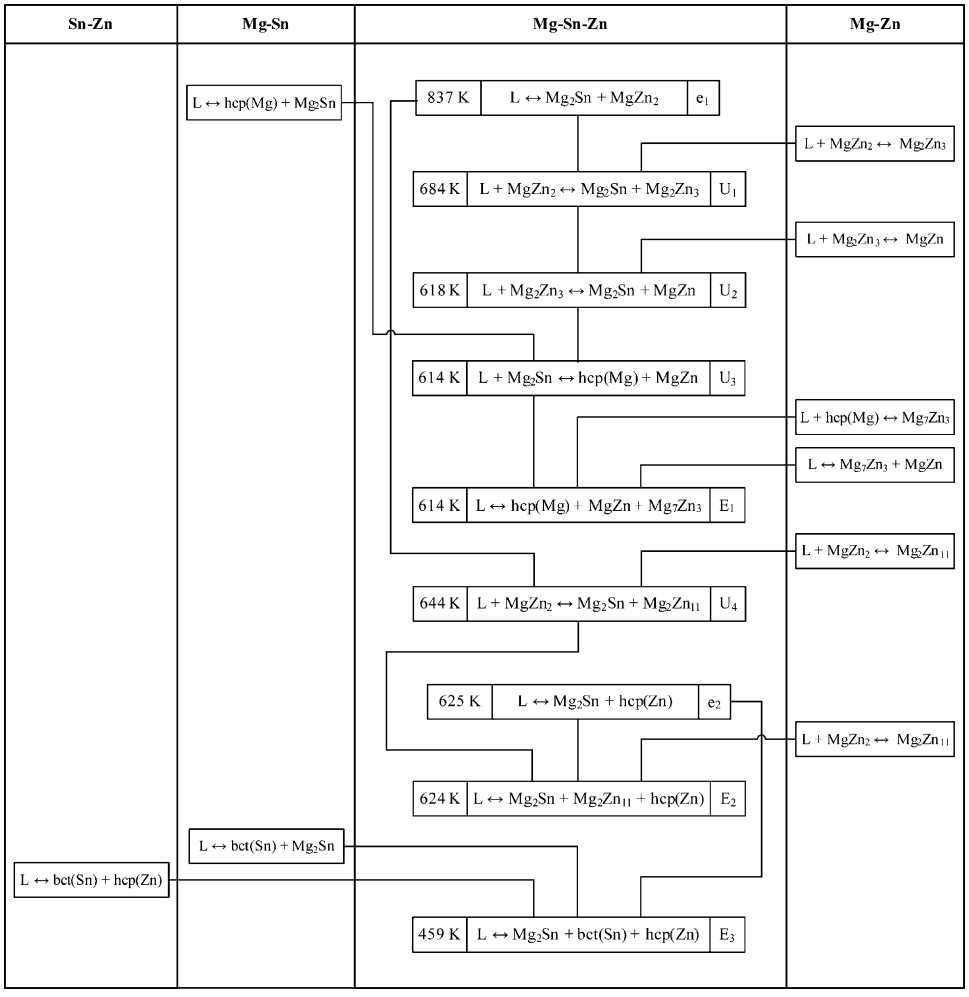

Fig. 12. The reaction scheme of invariant reactions in the Mg–Sn–Zn ternary system.

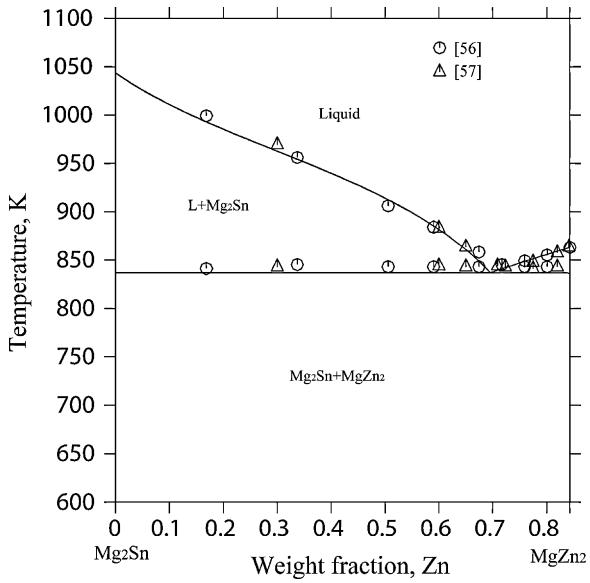

Fig. 13. Calculated vertical section of Mg_2Sn–Mg_2Zn with experimental data [56,57].

parameters of the liquid phase in the Mg–Sn, Mg–Zn and Sn–Zn binary systems, respectively; ${}^{(i)}L^{L}_{Mg_2Sn,Zn}$, ${}^{(i)}L^{L}_{Mg,Mg_2Sn,Zn}$, ${}^{(i)}L^{L}_{Mg_2Sn,Sn,Zn}$, ${}^{(i)}L^{L}_{Mg,Mg_2Sn,Sn,Zn}$ and ${}^{(i)}L^{L}_{Mg,Sn,Zn}$, are ternary interactive parameters, but ${}^{(i)}L^{L}_{Mg_2Sn,Zn}$ and ${}^{(i)}L^{L}_{Mg,Sn,Zn}$, are only used in the present optimization and others are set to be zero due to lack of experimental information in liquid ternary alloys.

On the other hand, the substitutional solution model is employed to describe the solid solution phases, hcp(Mg), bct(Sn) and hcp(Zn), respectively. The molar Gibbs energy of the solution phase ϕ (ϕ = hcp(Mg), bct(Sn) and hcp(Zn)) can be expressed as:

$$G_m^{\phi} = x_{Mg}{}^0G_{Mg}^{\phi} + x_{Sn}{}^0G_{Sn}^{\phi} + x_{Zn}{}^0G_{Zn}^{\phi} + RT(x_{Mg}\ln x_{Mg} + x_{Sn}\ln x_{Sn} + x_{Zn}\ln x_{Zn}) + {}^{E}G_m^{\phi} \quad (6)$$

where R is the gas constant, x_{Mg}, x_{Sn} and x_{Zn} are the mole fractions of Mg, Sn and Zn, respectively, and ${}^{E}G_m^{\phi}$ is the excess Gibbs energy expressed by the Redlich–Kister–Muggianu expression [61,62]:

$$\begin{aligned} {}^{E}G_m^{\phi} = {} & x_{Mg}x_{Sn}\sum_{i=0}^{n} {}^{i}L^{\phi}(x_{Mg}-x_{Sn})^i + x_{Mg}x_{Zn}\sum_{i=0}^{n} {}^{i}L^{\phi}(x_{Mg}-x_{Zn})^i \\ & + x_{Sn}x_{Zn}\sum_{i=0}^{n} {}^{i}L^{\phi}(x_{Sn}-x_{Zn})^i + x_{Mg}x_{Sn}x_{Zn}(x_{Mg}{}^{(0)}L^{\phi}_{Mg,Sn,Zn} \\ & + x_{Sn}{}^{(1)}L^{\phi}_{Mg,Sn,Zn} + x_{Zn}{}^{(2)}L^{\phi}_{Mg,Sn,Zn}) \end{aligned} \quad (7)$$

where ${}^{(i)}L^{\phi}_{Mg,Sn}$, ${}^{(i)}L^{\phi}_{Mg,Zn}$ and ${}^{(i)}L^{\phi}_{Sn,Zn}$ are binary interaction parameters in the Mg–Sn, Mg–Zn and Sn–Zn binary systems, respectively. The ternary interactive parameters, ${}^{(i)}L^{\phi}_{Mg,Sn,Zn}$, are set to zero for the solid solution phases (hcp(Mg), bct(Sn) and hcp(Zn)) due to lack of experimental data in the present work.

4.3. Intermetallic compounds

In the Mg–Sn binary system, the intermetallic compound Mg_2Sn is treated as a stoichiometric compound because of its narrow homogeneity range. Since the heat capacity and heat content of Mg_2Sn was determined by Jelinek et al. [53] and Morishita and Koyama [54], the Gibbs energy of Mg_2Sn can be given as:

$$G^{Mg_2Sn} = a_1 + b_1\cdot T + c_1\cdot T\ln T + d_1\cdot T^2 + e_1\cdot T^{-1} + f_1\cdot T^3 \quad (8)$$

where the parameters a_1 to f_1 are to be optimized in the present work.

According to the experimental results measured by Otani [56] and Gödecke and Sommer [57], there is no solubility of Sn in Mg_7Zn_3 and Mg_2Zn_3. The solubilities of Sn in $MgZn_2$ at 613 K and 840 K along the Mg_2Sn–$MgZn_2$ vertical section are 0.6 wt.% and 0.7 wt.%, respectively [57]. The solubilities of Zn in Mg_2Sn along the Mg_2Sn–$MgZn_2$ and Mg_2Sn–Zn vertical sections are 0.2 wt.% and about 0.1 wt.%, respectively [57]. However, Otani [56] reported the higher solubility of Zn in Mg_2Sn (up to about 5 wt.%), which are not convincible. In addition, the solubility of Sn in other Mg–Zn intermetallic compounds (MgZn, Mg_2Zn_{11}) was not studied. Therefore, the solubilities of Sn in Mg_7Zn_3, Mg_2Zn_3, $MgZn_2$, MgZn and Mg_2Zn_{11} as well as the solubility of Zn in Mg_2Sn were not considered in the present work.

5. Results and discussion

Using the compatible lattice stabilities of the elements Mg, Sn and Zn compiled by Dinsdale [58], the model parameters for various phases in the Mg–Sn–Zn ternary system were optimized using the PARROT module in the Thermo-calc® software package developed by Sundman et al. [14]. This module works through minimizing the square sum of the differences between experimental data and calculated values. During the present optimization procedure, each set of the experimental data was given a certain weight according to the reliability and compatibility of the experimental data. Thermodynamic parameters in the Mg–Sn–Zn ternary system used and obtained finally in the present work are summarized in Table 1. The calculated invariant reactions in the Mg–Sn binary system and the Mg–Sn–Zn ternary system are given in Tables 2 and 3, respectively. It can be seen that the reasonable agreement is achieved between the calculated results and the experimental data.

5.1. The Mg–Sn binary system

Fig. 3 shows the calculated phase diagram of the Mg–Sn binary system. The comparison of calculated phase diagram with the experimental data is given in Fig. 4. Enlarged parts of the Mg–Sn

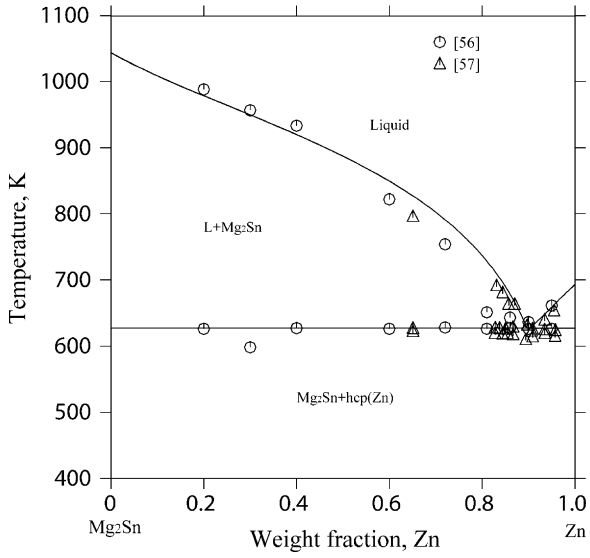

Fig. 14. Calculated vertical section of Mg_2Sn–Zn with experimental data [56,57].

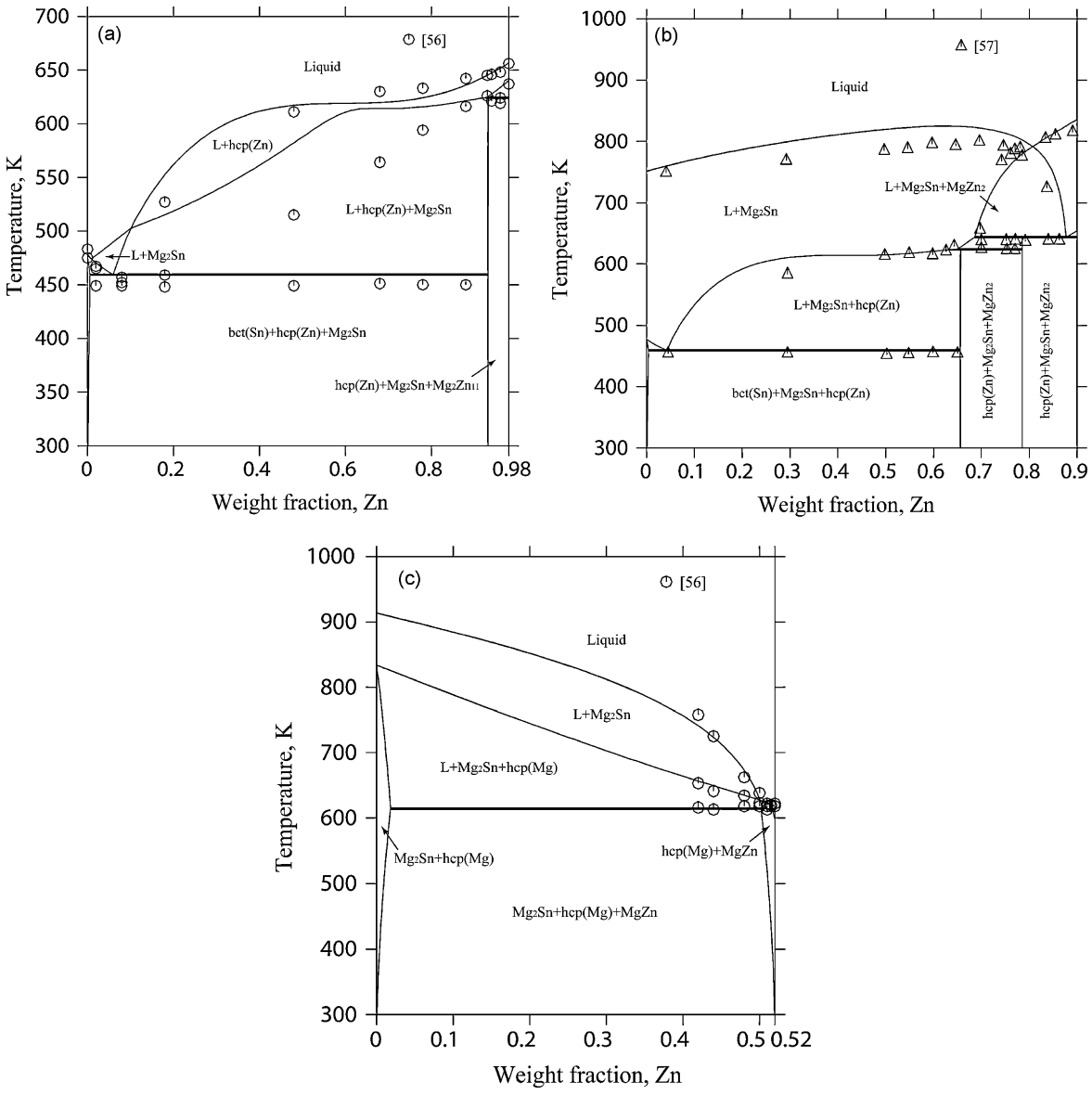

Fig. 15. Calculated vertical sections at the different Mg compositions in the Mg–Sn–Zn ternary system with experimental data [56,57]. (a) 2 wt.% Mg; (b) 10 wt.% Mg; (c) 48 wt.% Mg.

phase diagram in both Mg-rich and Sn-rich parts with the experimental data are further shown in Fig. 5. The calculated liquidus of hcp(Mg) and Mg_2Sn agree well with more reliable experimental data in Refs. [28–30]. The calculated liquidus of bct(Sn) phase and the solidus of hcp(Mg) phase are also consistent with the experimental data [25–35]. The calculated temperatures and compositions of invariant reactions are compared with the experimental data [26–32,34,35,45,46] and the assessed values by Fries and Lukas [23] in Table 2. As can be seen, the calculated results including liquidus, solidus and temperatures and compositions of invariant reactions are in good agreement with most of the experimental data and the assessed results [23].

The calculated enthalpy of mixing of liquid Mg–Sn alloys is compared with the experimental data [37–39] and the assessed results by Fries and Lukas [23] at different temperatures in Fig. 6. The present calculated results agree well with the experimental data [37,39] as well as the calculated results [23] and also show temperature dependency of enthalpy mixing of liquid alloys, while there is a slight discrepancy between the calculated values and the experimental ones [38].

Fig. 7 presents the comparison of the calculated activities of Mg in the liquid Mg–Sn alloys with the experimental data [42,45–47] and the assessed results by Fries and Lukas [23] at 1073 K. It can be seen that the calculated activities of Mg in liquid Mg–Sn alloys are in good agreement with the measured experimental data [45–47] and the calculated results [23], but show only a small discrepancy in the Mg-rich part compared with the experimental data reported by Sharma [42].

The enthalpies of formation of solid Mg–Sn alloys and intermetallic compound Mg_2Sn in the Mg–Sn binary system at 298 K were calculated as given in Fig. 8. As can be seen, the present calculated enthalpy of formation of solid Mg–Sn alloys is in good agreement with the measured experimental data [48,50] and the assessed results by Fries and Lukas [23], but show some deviation from the experimental data reported by Nayak and Oelsen [49]. The calculated enthalpy of formation of Mg_2Sn agrees with experimental data [39,48–52]. Figs. 9 and 10 show the calculated heat capacity and heat content of Mg_2Sn in comparison with the experimental data [39,53,54] and the assessed results by Fries and Lukas [23], respectively. The calculate heat capacity

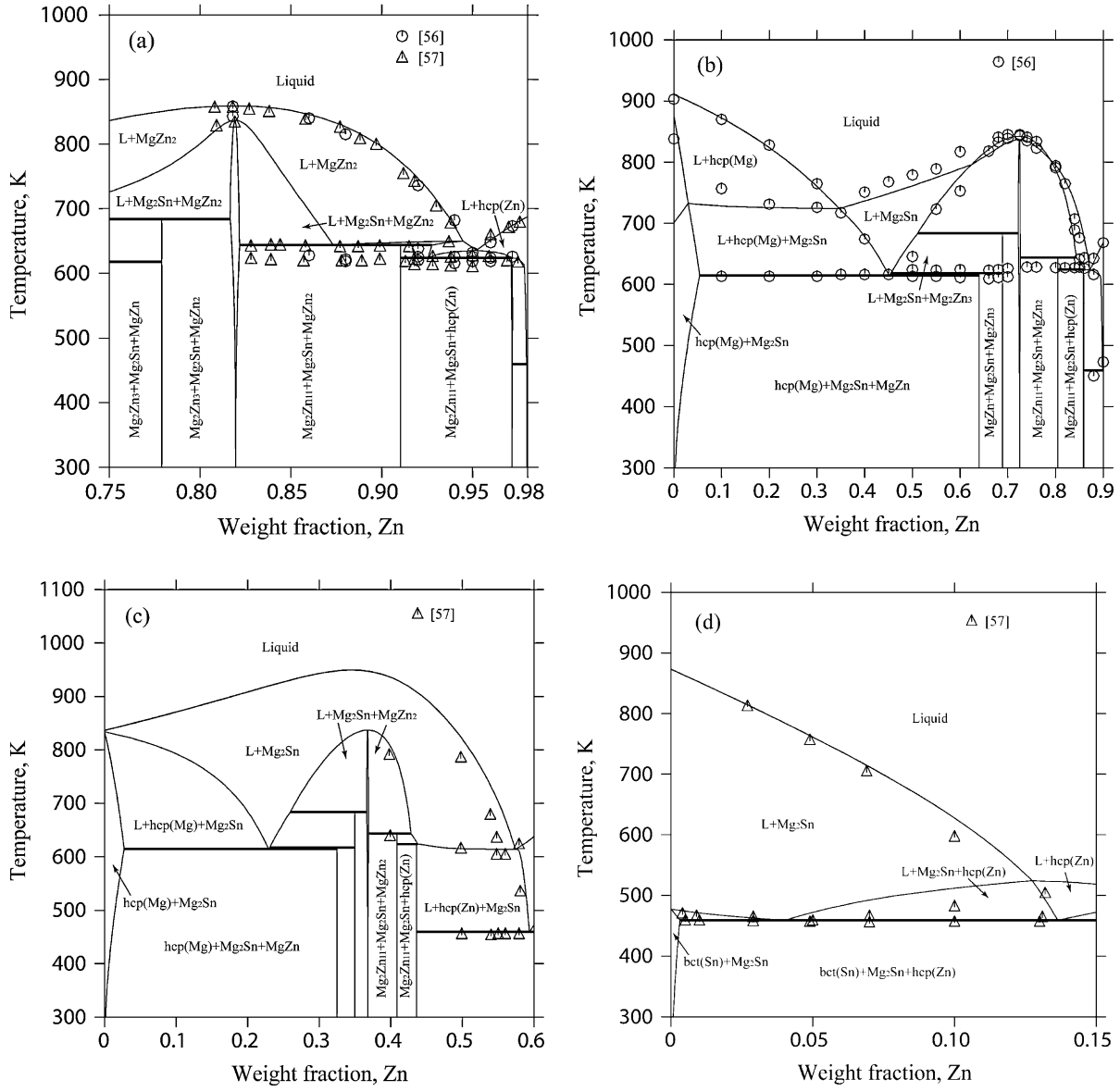

Fig. 16. Calculated vertical sections at the different Sn compositions in the Mg–Sn–Zn ternary system with experimental data [56,57]. (a) 2 wt.% Sn; (b) 10 wt.% Sn; (c) 40 wt.% Sn; (d) 85 wt.% Sn.

agrees well with the experimental data [53,54] at high temperature, while shows the slight deviation at low temperature. It can be seen that the excellent agreement is achieved between the calculated heat content of Mg_2Sn and the experimental data [39,54]. However, the calculated heat capacity by Fries and Lukas [23] at low temperature deviates unreasonably from the experimental data [53,54] and the present calculated results. The similar case is also shown in the comparison of the calculated heat content of Mg_2Sn by Fries and Lukas [23] with the experimental data [54] and the present calculated results. Therefore, the present assessed thermodynamic parameters of Mg_2Sn are much more reasonable and better than those of Fries and Lukas [23].

5.2. The Mg–Sn–Zn ternary system

Fig. 11 shows the calculated liquid projection of the Mg–Sn–Zn ternary system. The reaction scheme of the invariant reactions in the Mg–Sn–Zn ternary system is given in Fig. 12. The corresponding temperatures and compositions of the invariant reactions are given in Table 3. As can be seen, the liquid projection is dominated by the region of the primary crystallization for Mg_2Sn because of its high stability. The invariant reactions (E_2, E_3, U_4, e_1 and e_2) in the Mg_2Sn–$MgZn_2$–Zn–Sn part are in good agreement with the reported experimental results [56,57]. In the Mg_2Sn–$MgZn_2$–Mg part, the calculated results show that there are four invariant reactions, U_1, U_2, U_3 and E_1, which need to be confirmed in the further experiments.

The calculated vertical sections of Mg_2Sn–Mg_2Zn and Mg_2Sn–Zn are compared with the experimental data [56,57] in Figs. 13 and 14, respectively. As mentioned experimental results in Refs. [56,57], these two vertical sections are pseudobinary eutectic systems. It is evident that the calculated phase boundaries are in good agreement with the experimental data [56,57].

The calculated vertical sections at the different compositions of Mg, Sn and Zn, are presented in Figs. 15–17, respectively. In Fig. 15, the calculated vertical sections at 10 wt.% Mg and 48 wt.% Mg are consistent with the experimental results [56,57], while the

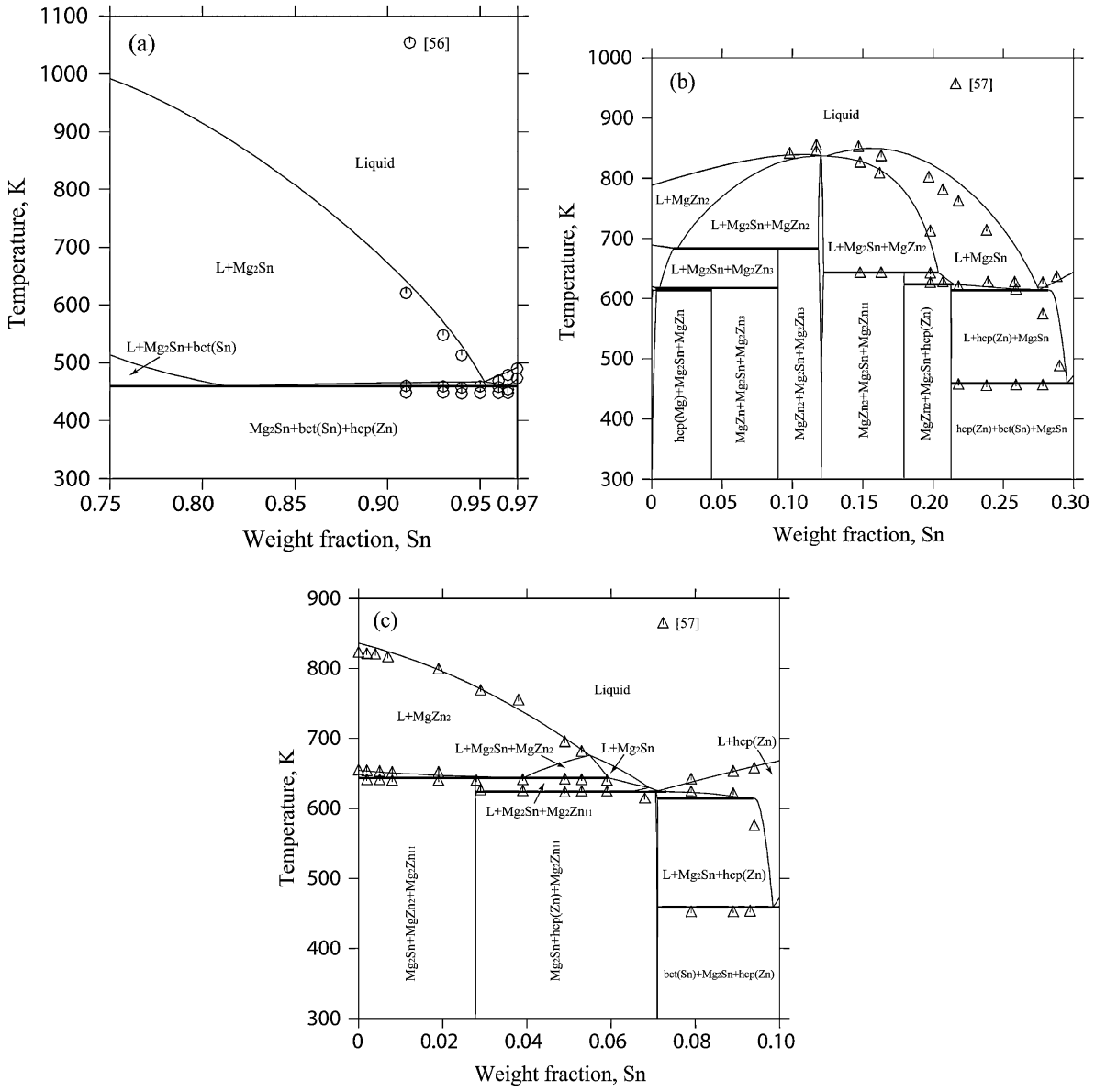

Fig. 17. Calculated vertical sections at the different Zn compositions in the Mg–Sn–Zn ternary system with the experimental data [56,57]. (a) 3 wt.% Zn; (b) 70 wt.% Zn; (c) 90 wt.% Zn.

calculated phase boundary for the vertical section of 2 wt.% Mg shows a slight deviation from the experimental data [56]. This deviation may result from the high stability of Mg_2Sn. However, since the experimentally reported solubility of Zn in Mg_2Sn is incomplete and inconsistent, Mg_2Sn is only modeled as a stoichiometric compound. Therefore, no thermodynamic parameters can be used to modify the stability of Mg_2Sn in the Mg–Sn–Zn ternary system. In the present work, other efforts have also been made to reproduce the phase boundary between L + hcp(Zn) and L + hcp(Zn) + Mg_2Sn in the 2 wt.% Mg section. However, it should be noticed that the calculated phase boundary is not sensitive to the most ternary parameters because this section is very close to phase diagram of the Sn–Zn binary system. The present authors suggest further experimental investigations to determine this vertical section and the solubility of Zn in Mg_2Sn. Fig. 16 compares the calculated vertical sections at 2 wt.% Sn, 10 wt.% Sn, 40 wt.% Sn and 85 wt.% Sn with the experimental data [56,57]. The calculated vertical sections at 3 wt.% Zn, 70 wt.% Mg and 90 wt.% Zn are illustrated in Fig. 17. It can be seen that the calculated results agree well with the experimental data [56,57] from Figs. 16 to 17.

6. Conclusions

The Mg–Sn binary system was re-optimized using the CALPHAD method through Thermo-calc® software package. A set of self-consistent parameters for the Mg–Sn binary system was obtained, which can be used to reproduce satisfactorily most experimental data including thermodynamic property and phase diagram. Combined with the previous assessments of the Mg–Zn and Sn–Zn binary systems, the thermodynamic modeling of the Mg–Sn–Zn ternary system was performed. Liquidus projection and several vertical sections of this ternary system were calculated. The calculated results are in good agreement with the reported experimental data.

Acknowledgements

This work was supported financially by Scientific Research Foundation of Hunan Province Department of Land & Resources, China (Grant No. 2008K 22), Geology Exploration Foundation of Hunan Province Department of Land & Resources, China, and Scientific Research Foundation for Advanced Talents in Central South University of Forestry and Technology as well as National Natural Science Foundation of China (Grant No. 50731002).

References

[1] M. Bamberger, G. Dehm, Annu. Rev. Mater. Res. 38 (2008) 505–533.
[2] Z.H. Chen, J.H. Chen, Front. Mater. Sci. China 2 (2008) 1–8.
[3] D.J. Li, X.Q. Zeng, J. Dong, C.Q. Zhai, W.J. Ding, J. Alloys Compd. 468 (2009) 164–169.
[4] J. Zhang, R.L. Zuo, Y.X. Chen, F.S. Pan, X.D. Luo, J. Alloys Compd. 448 (2008) 316–320.
[5] J.F. Nie, K. Oh-ishi, X. Gao, K. Hono, Acta Mater. 56 (2008) 6061–6076.
[6] B. Rashkova, W. Prantl, R. Görgl, J. Keckes, S. Cohen, M. Bamberger, G. Dehm, Mater. Sci. Eng. A 494 (2008) 158–165.
[7] I.-H. Jung, D.H. Kang, W.-J. Park, N.J. Kim, S.H. Ahn, Int. J. Mater. Res. 98 (2007) 807–815.
[8] J. Gröbner, A. Janz, A. Kozlov, D. Mirkovic, R. Schmid-fetzer, M. Ohno, JOM 60 (2008) 32–38.
[9] Y.-B. Kang, C. Aliravci, P.J. Spencer, G. Eriksson, C.D. Fuerst, P. Chartrand, A.D. Pelton, JOM 61 (2009) 75–82.
[10] M. Bamberger, J. Mater. Sci. 41 (2006) 2821–2829.
[11] I.-H. Jung, W.-J. Park, S.H. Ahn, D.H. Kang, N.J. Kim, Magnes. Technol. (2006) 457–461.
[12] L. Kaufman, H. Bernstein, Computer Calculation of Phase Diagrams, Academic Press, New York, 1970.
[13] N. Saunders, A.P. Modwnik, CALPHAD-A Comprehensive Guide, Pergamon, Lausanne, Switzerland, 1998.
[14] B. Sundman, B. Jansson, J.O. Anderson, CALPHAD 9 (1985) 153–190.
[15] R. Agarwal, S.G. Fries, H.L. Lukas, G. Petzow, F. Sommer, T.G. Chart, G. Effenberg, Z. Metallkd. 83 (1992) 216–223.
[16] P. Liang, T. Tarfa, J.A. Robinson, S. Wagner, P. Ochin, M.G. Harmelin, H.J. Seifert, H.L. Lukas, F. Aldinger, Thermochim. Acta 314 (1998) 87–110.
[17] P. Liang, H.J. Seifert, H.L. Lukas, G. Ghosh, G. Effenberg, F. Aldinger, CALPHAD 22 (1998) 527–544.
[18] M. Ohno, R. Schmid-Fetzer, Int. J. Mater. Res. 97 (2006) 526–532.
[19] H.Y. Qi, G.X. Huang, R.D. Liu, K. Zhang, L.B. Liu, Z.P. Jin, J. Alloys Compd. 497 (2010) 336–343.
[20] B.-J. Lee, CALPHAD 20 (1996) 471–480.
[21] H. Ohtani, M. Miyashita, K. Ishida, J. Japan Inst. Met. 63 (1999) 685–694.
[22] A.A. Nayeb-Hashemi, J.B. Clark, Bull. Alloy Phase Diagram 5 (1984) 466–476.
[23] S.G. Fries, H.L. Lukas, J. Chim. Phys. 90 (1993) 181–187.
[24] A. Kozlov, M. Ohno, R. Arroyave, Z.K. Liu, R. Schmid-Fetzer, Intermetallics 16 (2008) 299–315.
[25] C.T. Heycock, F.H. Neville, J. Chem. Soc. 57 (1890) 376–392.
[26] G. Grube, Z. Anorg. Chem. 46 (1905) 76–84.
[27] N.S. Kurnakow, N.J. Stepanow, Z. Anorg. Chem. 46 (1905) 177–192.
[28] W. Hume-Rothery, J. Inst. Met. 35 (1926) 336–347.
[29] G.V. Raynor, J. Inst. Met. 6 (1940) 403–426.
[30] A. Steiner, E. Miller, L. Komarek, Trans. Met. Soc. AIME 230 (1964) 1361–1367.
[31] A.K. Nayak, W. Oelsen, Trans. Indian Inst. Met. 21 (1968) 15–20.
[32] A.K. Nayak, W. Oelsen, Trans. Indian Inst. Met. 22 (1969) 53–58.
[33] J. Ellmer, K.E. Hall, R.W. Kamphefner, J. Pfeifer, V. Stamboni, C.D. Graham, Metall. Trans. 4 (1973) 889–891.
[34] G. Grube, H. Vosskühler, Z. Electrochem. 40 (1934) 566–570.
[35] H. Vosskühler, Metallwirtschaft 20 (1941) 805–808.
[36] H. Nishinura, K. Tanaka, Trans. Inst. Min. Metall. Alumni Assoc. 10 (1940) 343–350.
[37] M. Kawakami, Sci. Rep. Res. Inst. Toholu Univ. 19 (1930) 521–549.
[38] A.K. Nayak, W. Oelsen, Trans. Indian Inst. Met. 24 (1971) 22–28.
[39] F. Sommer, J.J. Lee, B. Predel, Z. Metallkd. 71 (1980) 818–821.
[40] V.N. Eremenko, G.M. Lukashenko, Ukr. Khim. Zh. 29 (1963) 896–900.
[41] J.M. Eldridge, E. Miller, K.L. Komarek, Trans. Met. Soc. AIME 239 (1967) 775–781.
[42] R.A. Sharma, J. Chem. Thermodyn. 2 (1970) 373–389.
[43] J.M. Eldridge, E. Miller, K.L. Komarek, Trans. Met. Soc. AIME 236 (1966) 114–121.
[44] S. Ashtakala, L.M. Pidgeon, Can. J. Chem. 40 (1962) 718–727.
[45] C.A. Eckert, R.B. Irwin, J.S. Smith, Met. Trans. B 14 (1983) 451–458.
[46] J.J. Egan, J. Nucl. Mater. 51 (1974) 30–35.
[47] Z. Moser, W. Zakulski, Z. Panek, M. Kucharski, L. Zabdyr, Met. Trans. B 21 (1990) 707–714.
[48] O. Kubaschewski, Z. Elektrochem. 45 (1939) 732–740.
[49] A.K. Nayak, W. Oelsen, Trans. Indian Inst. Met. 24 (1971) 66–73.
[50] A. Borsese, G. Borzone, R. Ferro, R. Capelli, Z. Metallkd. 66 (1975) 226–227.
[51] O. Kubaschewski, E.L. Evans, Metallurgical Thermochemistry, Pergamon Press Ltd., London, 1956.
[52] P. Beadmore, B.W. Howlett, B.D. Lichter, M.B. Bever, Trans. Met. Soc. AIME 236 (1966) 102–108.
[53] F.J. Jelinek, W.D. Shickell, B.C. Gerstein, J. Phys. Chem. Solids 28 (1967) 267–270.
[54] M. Morishita, K. Koyama, J. Alloys Compd. 398 (2005) 12–15.
[55] N. Ogawa, T. Miki, T. Nagasaka, M. Hino, Mater. Trans. 43 (2002) 3227–3233.
[56] B. Otani, Tetsu to Hagane 19 (1933) 566–574.
[57] T. Gödecke, F. Sommer, Z. Metallkd. 85 (1994) 683–691.
[58] A.T. Dinsdale, CALPHAD 15 (1991) 317–425.
[59] F. Sommer, Z. Metallkd. 73 (1982) 72–76.
[60] R. Schmid-Fetzer, Y.A. Chang, CALPHAD 9 (1985) 363–382.
[61] O. Redlich, A.T. Kister, Ind. Eng. Chem. 40 (1948) 345–348.
[62] Y.M. Muggianu, M. Gambino, J.P. Bros, J. Chim. Phys. 72 (1975) 83–88.